**Article:**
Zeb, A, Hall, DA, Aslam, Z et al. (7 more authors) (2019) Structure-property relationships in the lead-free piezoceramic system $K_{0.5}Bi_{0.5}TiO_3$ - $BiMg_{0.5}Ti_{0.5}O_3$. Acta Materialia, 168. pp. 100-108. ISSN 1359-6454

https://doi.org/10.1016/j.actamat.2019.02.011

# Structure-Property Relationships in the Lead-free Piezoceramic System $K_{0.5}Bi_{0.5}TiO_3$ - $BiMg_{0.5}Ti_{0.5}O_3$

**Aurang Zeb[1,2], David A. Hall[3], Zabeada Aslam[3], Jennifer Forrester[1], Jing-Feng Li[4], Yizhe L. Li[3], Chiu C. Tang[5], Ge Wang[3], Fangyuan Zhu[6], Steven J. Milne[1]***

[1] School of Chemical and Process Engineering, University of Leeds, Leeds, LS2 9JT, United Kingdom.

[2] Department of Physics, Islamia College Peshawar, KP, Pakistan.

[3] School of Materials, University of Manchester, Manchester, M13 9PL, United Kingdom.

[4] State Key Laboratory of New Ceramics and Fine Processing, School of Materials Science and Engineering, Tsinghua University, Beijing 100084, China.

[5] Diamond Light Source Ltd, Harwell Science and Innovation Campus, Didcot, Oxfordshire, OX11 0DE, United Kingdom.

[6] Shanghai Institute of Applied Physics, Chinese Academy of Science, Shanghai, 201204, China.

* Corresponding Author: s.j.milne@leeds.ac.uk

## Abstract

Distinctive structure-property relationships are revealed in the relaxor ferroelectric ceramic solid solution, (1-x)$K_{0.5}Bi_{0.5}TiO_3$ - x$BiMg_{0.5}Ti_{0.5}O_3$: $0.02 < x < 0.08$. The constructed phase diagram and results of *in-situ* synchrotron X-ray diffraction provide explanations for temperature and electric field dependent anomalies in dielectric, ferroelectric and electromechanical properties. At room temperature a mixed phase tetragonal and pseudocubic phase field occurs for compositions $0 > x \leq 0.07$. As temperature rises to ≥ 150 °C, the ferroelectric tetragonal relaxor phase changes to a pseudocubic ergodic relaxor phase; this change in length scale of polar order is responsible for an inflection in relative permittivity - temperature plots. The transition is reversed by a sufficient electric field, thereby explaining the constricted form of polarisation-electric field loops measured at >150°C. It is also responsible for a change in slope of the strain-electric field (S-E) plots which are relatively linear in the ferroelectric regime i.e. at temperatures up to 150 °C, giving unipolar strains of 0.11 % at 20 °C and 0.14% at 150 °C (50 kV $cm^{-1}$ field). The additional contribution from the effect of the field-induced pseudocubic to tetragonal transition, generates strains of ~ 0.2 % at 185 °C. Unusual for a piezoelectric solid solution, the maximum strains and charge coefficients ($d_{33}$ =150 pC $N^{-1}$, 20 °C) do not coincide with a morphotropic or polymorphic phase boundary.

## 1. Introduction

Lead zirconate titanate (PZT) based ceramics are used in a wide range of sensor, actuator and transducer applications.[1] Environmental and health concerns surrounding the use of lead oxide have resulted in a search for lead-free alternatives. PZT is a solid solution between $PbZrO_3$ and $PbTiO_3$ in which a phase boundary exists between two ferroelectric phases, rhombohedral and tetragonal (possibly with a bridging monoclinic region).[1,2] This phase boundary is almost vertical on the $PbZrO_3$-$PbTiO_3$ phase diagram, and for this reason it is referred to as a *morphotropic* phase boundary (MPB), only showing significant curvature as temperature approaches the Curie point ($T_c$ ~ 370 °C). The coexistence of ferroelectric phases with differing symmetry and polar directions gives enhanced piezoelectric properties at the MPB due to ease of polarisation rotation. The temperature-insensitive nature of the MPB confers favourable temperature stability to the piezoelectric properties of PZT.[1] Despite its relatively high $T_c$ the maximum working temperature of most types of PZT is ~ 200-250 °C, presumably due to a combination of property degradation and instability under electrical and mechanical loading.[3,4] A range of chemical dopants, commonly classified as donors (*soft* PZT) or acceptors (*hard* PZT), are used to tailor the properties of PZT for specific applications.

Numerous lead-free piezoelectrics have been proposed.[5] In some cases, such as in some early reports of $Na_{0.5}K_{0.5}NbO_3$ (NKN) based systems, a relatively high value of piezoelectric coefficient ($d_{33}$) occurs because of phase co-existence at a polymorphic phase transition (PPT) between orthorhombic and tetragonal ferroelectric phases. The PPT is temperature- and composition-dependent and appears as an inclined boundary on the phase diagram, rather than the desired temperature-invariant near-vertical MPB.[6-8] For various NKN solid solutions, for example NKN-$LiTaO_3$, a reasonably high value of $d_{33}$ at room-temperature occurs in compositions for which the PPT occurs at room-temperature however properties degrade significantly as temperature changes. Many piezoelectric devices require stability in properties over a wide temperature range and this has prompted research into devising NKN-type solid solutions in which PPT temperatures are shifted to below room-temperature, as in NKN-7%$LiTaO_3$. This approach has been demonstrated to give stable properties over repeated thermal cycling.[7,11] Other workers have incorporated substituents that broaden the temperature range of the PPT, which still occurs within the anticipated working temperature range of the piezoelectric. The diffuse nature of the phase transition minimises the variability in measured properties, at least over a single heating cycle.[8-10]

Another promising group of lead-free piezoelectrics are based on $Na_{0.5}Bi_{0.5}TiO_3$ (NBT), a relaxor ferroelectric. The coherence length scales of polar order in a relaxor are much shorter than those in a

conventional ferroelectric, on the nanoscale rather than microscale. The nano-polar structure is generally thought to be due to compositional disorder in the perovskite lattice which prevents long-range ferroelectric domains forming on cooling from the paraelectric state, i.e. from temperatures above the Burns temperature, $T_B$. Chemical variability on the lattice-scale creates fluctuating electrostatic and strain fields that inhibit long range order of the dipoles that originate from off-centre A- and B-site ions within $AO_{12}$ and $BO_6$ polyhedra respectively. Below $T_B$, the rise in relative permittivity is consistent with an increase in polar order within nanoscale domains and increases in domain size as temperature falls. Eventually, on cooling the dynamics of field-induced dipole reorientation slow down, causing bulk polarization to decrease and creating a broad, frequency-dependent dielectric peak (at temperature $T_m$). On further cooling, a change from ergodic to non-ergodic relaxor (ferroelectric) behaviour occurs as the dipoles 'freeze'.

Lead-free piezoelectrics based on relaxor ferroelectrics such as NBT generally exhibit improved temperature stability of properties compared to many NKN-based counterparts. Binary solid solutions of NBT with $BaTiO_3$ (BT) or $K_{0.5}Bi_{0.5}TiO_3$ (KBT) display an MPB, and for this reason NBT-BT and NBT-KBT systems have attracted great interest.[13-18] Their $d_{33}$ values are in the range 122-176 pC/N for MPB NBT-BT compositions,[5] and 140-190 pC/N for NBT-KBT.[5,19-21] Strains of up to ~ 0.4 % in NBT-BT arise from a reversible field induced phase transition.[22] However modest depolarisation temperatures ($T_d$) for compositions with the best piezoelectric properties pose a significant drawback. Ceramics of NBT-BT near the MPB have $T_d$ values of 90-120°C.[5,23] Corresponding $T_d$ values are slightly higher for NBT-BKT, at 130-170°C.[5]

Ternary NBT based systems include NBT-KBT-BT,[24,25] typically with $d_{33}$ ~ 170 pC/N and $T_d$ ~ 162°C, and NBT-BT-NKN which develops 'giant' electromechanical bipolar strains up to ~ 0.45% in the MPB region due to a reversible electric field-induced phase transformation at high drive fields, as does NBT-KBT-NKN.[26-28] The field-induced transformation gives rise to a characteristic discontinuity in S-E plots and increased strain hysteresis. For actuator applications, narrow S-E loops with low hysteresis are preferred in order to provide improved positional accuracy and to minimize self-heating problems and possible depolarisation.

There is limited literature on KBT-based piezoelectrics.[29-33] Although unmodified KBT exhibits relatively low field-induced strain values, it has attracted interest because of its high depolarisation temperature, $T_d$ ~ 250 °C. Many electromechanical device applications involve high operating temperatures, for example 150 °C for fuel injection systems.[29,30] However, costly hot pressing is required to fabricate high density KBT and to achieve suitable levels of strain, for example a strain of 0.04% is reported for conventionally fabricated ceramics and ~ 0.12% for hot pressed KBT (at 80 kV/cm).[29,30] By modifying KBT with $Bi(Mg_{0.5}Ti_{0.5})O_3$ (BMT), it was shown that improved values of $d_{33}$ and room-temperature electromechanical bipolar strains could be obtained for conventionally processed ceramics.

[31,32] This article reports structure-property relationships in KBT-BMT ceramics and reveals reasons for the temperature- and field-dependent discontinuities in properties. Unusually for a piezoelectric solid solution, electromechanical property enhancements are not correlated with a phase boundary, instead maximum charge coefficients and field induced strains occur within a two phase tetragonal and pseudocubic region at approximately a 50/50 ratio of the two phases.

## 2. Experimental Procedures

Sample compositions were prepared, using conventional solid state processing, according to the formula $(1-x)K_{0.5}Bi_{0.5}TiO_3$ - $xBi(Mg_{0.5}Ti_{0.5})O_3$ [KBMT] for the compositional range $0 \leq x \leq 0.12$. The assumed solid solution formula is: $K_{(0.5-0.5x)}Bi_{(0.5+0.5x)}Ti_{(1-0.5x)}Mg_{(0.5x)}O_3$, with $K^+$ and $Bi^{3+}$ on A-sites and $Ti^{4+}$ and $Mg^{2+}$ occupying B- sites of the perovskite lattice. The reagents were $K_2CO_3$ (Sigma Aldrich, 99% purity), $Bi_2O_3$ (Sigma Aldrich, 99.9%), MgO (Alfa Aesar, 99.9%) and $TiO_2$ (Sigma Aldrich, 99.9%). After drying overnight at 250 °C and cooling to room-temperature, the powders were stored in a desiccator under reduced pressure and subsequently weighed in the appropriate ratios. The powders were then ball milled with $ZrO_2$ grinding media in isopropanol for 24 h; the dried slurries were passed through a 300 μm mesh nylon sieve and calcined at 850 °C for 3 h in alumina crucibles with heating and cooling ramp rates of 300 °C/h. After calcination, the sieved powders were milled again for 24 h and 1 wt % binder was added (Ciba Glascol HA4: Ciba Speciality Chemicals, Bradford, UK). Pellets of 10 mm diameter and ~ 1.5 mm thickness were pressed uniaxially at 100 MPa in a steel die, followed by cold isostatic pressing at 200 MPa. The binder was burned out by heating at 50 °C/h to 550 °C, followed by heating at 300 °C/h to sintering temperatures of 1050 °C to 1100 °C with a 4 h dwell period. There was a narrow range of temperatures in which densification could be obtained, above which partial melting occurred. Pellets were embedded in a powder of the same composition during sintering to minimise losses due to volatilisation of $K_2O$ and $Bi_2O_3$.

High-resolution synchrotron X-ray powder diffraction (SXPD) measurements at room-temperature were performed on beamline I11[34] at the Diamond Light Source, UK. Powder samples were prepared by crushing and grinding the as-sintered ceramic pellets, followed by loading into glass capillaries with a diameter of 0.3 mm. SXPD patterns were obtained using a photon energy of 15 keV, corresponding to a wavelength of 0.825838(10) Å, and the resulting diffraction patterns were recorded using multi-analyser crystal (MAC) detectors at room-temperature. Calibrated was performed using a high quality Si powder standard, and the step-size was 0.001°2θ. Full-pattern refinement was carried out using the Rietveld analysis program GSAS.[35]

High temperature X-ray diffraction (XRD) patterns were recorded using laboratory XRD, with $CuK_\alpha$ radiation $\lambda = 1.54056$ Å, and a scan speed 1°/min over the temperature range from 25 °C to 400 °C using a PANalytical X'Pert Pro MPD diffractometer (Philips, Almelo, Netherlands) fitted with a HTK 1200 oven

and TCU 1000 controller (Paar Physica): peak profile fitting was performed using the X'Pert Highscore Plus software.

In-situ sychrotron XRD experiments were carried out in transmission on beamline I15 of the Diamond Light Source, using a high energy monochromatic x-ray beam having a photon energy of 76 keV ($\lambda$ = 0.16314 Å) and a cross-section of approximately 70 μm. Test specimens were prepared in the form of square-ended beams having dimensions ~ 1 mm x 1 mm x 5 mm, by diamond machining. 2-D XRD images were recorded using a Perkin-Elmer XRD1621 flat-panel detector, with a collection time of 10 s. Subsequently, the detector was calibrated with a $LaB_6$ standard powder and 1-D diffraction patterns corresponding to a range of azimuthal angles, $\psi$, were obtained using DAWN [42]. A Matsusada ECA-10 high voltage amplifier was employed to apply an electric field between the upper and lower faces of the test specimen, perpendicular to the X-ray beam, with the sample being immersed in silicone oil to avoid electrical arcing.

For electrical measurements, the sintered pellets were ground to ~ 1 mm thickness and silver paste (Agar Scientific) was applied to opposite parallel faces; the pellets were heated in a furnace at 550 °C for 10 min to form electrodes. Relative permittivity and loss tangent were recorded as a function of temperature using an impedance analyser (HP Agilent, 4192A Hewlett Packard, Santa Clara, CA), from 25°C to 600°C. For piezoelectric testing, samples were poled in silicone oil by applying a dc field of 40-60 kV/cm at a temperature of ~ 80 ºC for 20 min. The piezoelectric charge coefficients, $d_{33}$, were measured 24 h after poling, using the Berlincourt technique (Piezotest meter PM 300; Piezotest, London, UK). Strain-electric field and polarization-electric field data were obtained using a ferroelectric analyzer (aixACCT TE1000, aixACCT Systems GMbH, Aachen, Germany) at various temperatures, with a frequency of 1 Hz. The equipment used to measure high-temperature strains permitted a maximum drive field of 50 kV/cm. Electrical resistivity, $\rho$, was measured using a Kiethley Electrometer: $\rho_{300\,C}$ was ~ $2 \times 10^9$ Ω m.

High temperature ferroelectric hysteresis measurements were carried out in a silicone oil bath over the temperature range from 25-175°C using a HP33120A function generator in combination with a HVA1B high voltage (±5 kV) amplifier (Chevin Research, Otley, UK). The measured electric field-time and current-time waveforms were processed to yield near-saturated polarization-electric field (P-E) loops in the high (super-coercive) field region and effective dielectric properties ($\varepsilon_r'$, $\varepsilon_r''$, tanδ) in the medium (sub-coercive) field region using the method described previously.[38-40] Scanning electron microscopy (SEM) was carried out using a Hitachi SU 8230 FESEM. Transmission electron microscopy (TEM) was performed using an FEI Tecnai field emission gun (FEG)-transmission electron microscope operating at 200 kV and fitted with an Oxford Instruments 80 mm X-Max SDD energy dispersive X-ray (EDX) spectrometer and a Gatan Orius

SC600A CCD camera; non-ambient TEM was carried out with a hot-stage sample holder using the same instrument.

## 3. Results and Discussion

### 3.1 Phase Analysis

Full-pattern refinement of high resolution synchrotron X-ray powder diffraction (SXPD) data on crushed sintered pellets at room-temperature confirm the KBT end-member to be single phase tetragonal, $P4mm$. Modification with $x = 0.02$ BMT (the lowest BMT content studied) generates a mixed tetragonal and cubic $Pm\bar{3}m$ phase, as indicated by the fitted parameters listed in Table 1. The mixed phase region extends to $x \leq 0.07$, with a rising proportion of cubic phase with increasing $x$ (Table 1). Composition $x = 0.08$ is single phase cubic, while $x = 0.1$ and 0.12 are cubic with minor amounts of $Bi_4Ti_3O_{12}$ present.

**Table 1. Summary of crystallographic parameters and phase fractions determined from full pattern refinement of high resolution SXPD data.**

| Composition | Lattice parameter *a* (Tetragonal) Å | Lattice parameter *c* (Tetragonal) Å | *c*/*a* ratio | Lattice parameter *a* (Cubic ) Å | Phase fraction % | $wR_p$ % | $R_p$ % |
|---|---|---|---|---|---|---|---|
| KBT | 3.92365(4) | 4.00746(5) | 1.02136(3) | - | 100% T | 9.34 | 7.36 |
| 0.98KBT-0.02BMT | 3.92493(5) | 4.00169(2) | 1.01956(4) | 3.94640(3) | 59.1(2)T/40.9(2)C | 8.63 | 6.42 |
| 0.97KBT-0.03BMT | 3.92597(4) | 3.99814(2) | 1.01838(4) | 3.94739(3) | 52.4(2)T/47.6(2)C | 7.76 | 5.58 |
| 0.96KBT-0.04BMT | 3.92777(6) | 3.99553(1) | 1.01719(4) | 3.94839(4) | 42.8(2)T/57.2(2)C | 7.73 | 5.80 |
| 0.93KBT-0.07BMT | 3.93707(2) | 3.98470(3) | 1.01210(2) | 3.95061(2) | 25.5(2)T/74.5(2)C | 7.69 | 5.75 |

A full pattern Rietveld refinement of the $x$ = 0.03 composition, which displays the best electromechanical properties, is shown in Figure 1a, along with detail of the {110}, {111} and {200} diffraction profiles, Figure 1b. Refinement parameters for the various KBMT compositions are shown in Table S1, Supporting Information. The tetragonal lattice parameters showed a slight contraction along the *c*-axis and an expansion of the *a*-axis with increasing BMT content: the tetragonal *c*/*a* ratio decreased from 1.02136(3) for KBT ($x$ = 0.00) to 1.01838(4) at $x$ = 0.03 KBMT, Table 1 and Figure S1, Supporting Information. The cubic lattice parameters increased marginally with increasing BMT content, Figure S1. Systematic variations in the lattice parameters of both phases as a function of x indicate that they each are solid solutions.

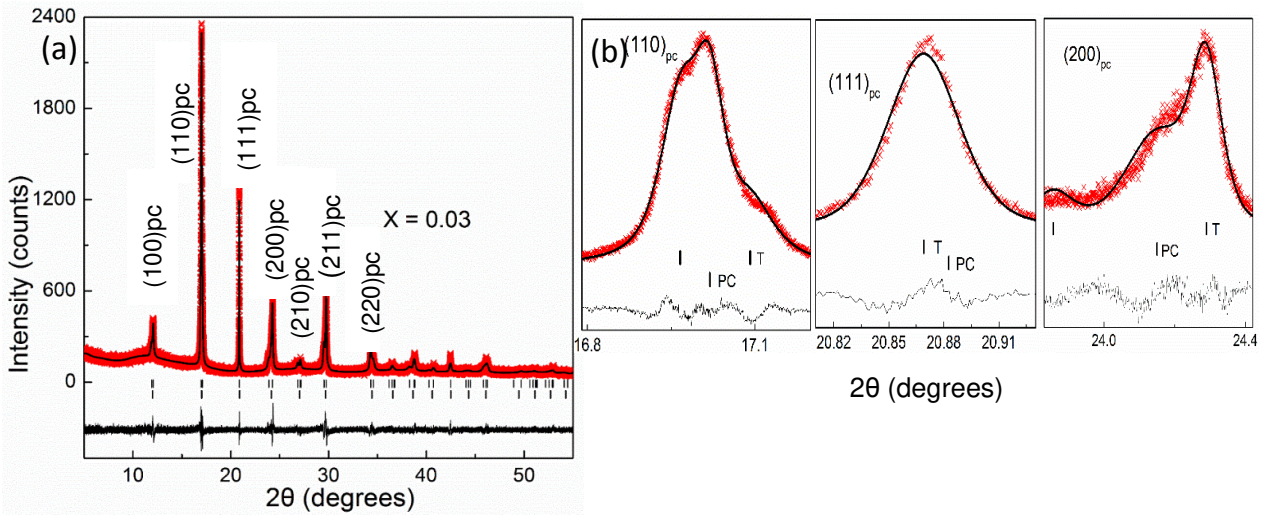


**Figure 1. a) SXPD full pattern refinement of $x$ = 0.03 KBMT, confirming the presence of tetragonal and cubic/pseudocubic phases ($hkl_p$), $R_p$ = 5.58%. b) Expanded view of the {110}, {111), and {200} diffraction profiles (PC denotes pseudocubic indices).**

The phase diagram for KBMT, as determined from SXPD data at 25 °C combined with laboratory XRD data, recorded over the temperature range 50-400 °C (at 25 °C increments), is shown in Figure 2; representative high temperature XRD patterns appear in Figure S2, Supporting Information. The KBT end-member is single phase tetragonal from 25 to 280 °C, becoming mixed tetragonal and cubic between 280 and 310 °C, above which it becomes single phase cubic ('$T_{ST}$' is used hereafter to signify the temperature of the structural transition to single phase cubic). The effect of incorporating BMT is to stabilise the mixed phase region to room-temperature for KBMT solid solution compositions with $0.02 \leq x \leq 0.07$. The $T_{ST}$ value for $x$ = 0.02 is similar to that of KBT ($x$ = 0), but then decreases with further increases in $x$, the sharpest fall occurring at $x > 0.06$; $T_{ST}$ reaches room-temperature (or below) at $x = 0.08$, as shown in Figure 2. Synchrotron XRD reported in Section 3.3 indicate the tetragonal to pseudocubic structural transition occurs at lower temperatures in dense sintered ceramics (Figure 2 relates to powders obtained by crushing sintered pellets). The $c$ and $a$ tetragonal lattice parameters of solid solution compositions converge with increasing temperature in the manner of a typical ferroelectric on approaching its Curie point, Figure S3,Supporting Information. Grain sizes were sub-micron with evidence of non-180° domains in some grains, Figure 3, consistent with the tetragonal phase identified by XRD.

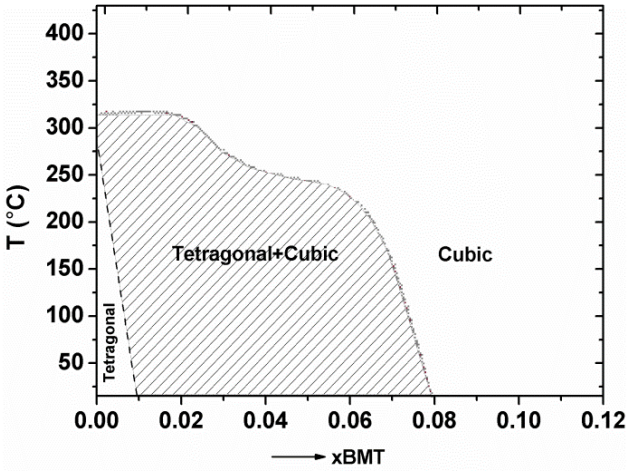


**Figure 2. Phase diagram for the KBMT ceramic system based on XRD of crushed sintered pellets. The phase indicated as cubic by XRD is subsequently shown to be pseudocubic (see text).**

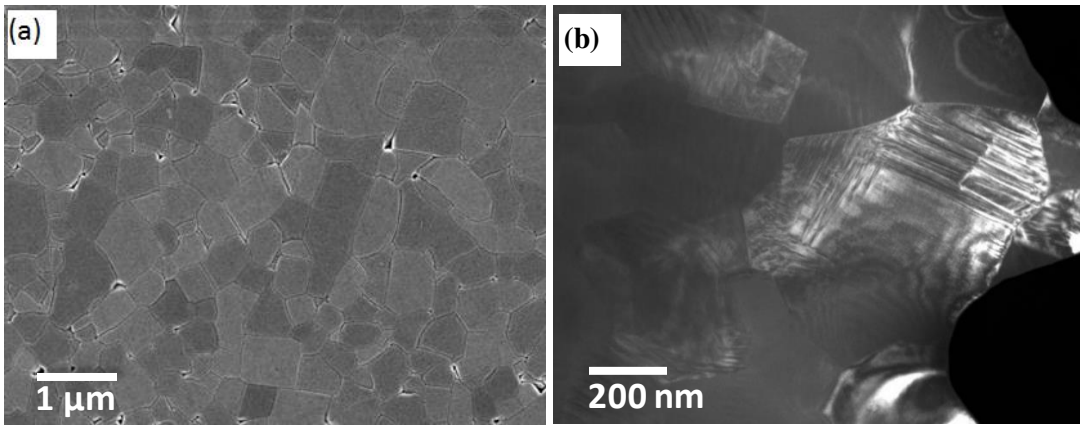


**Figure 3. a) SEM micrograph of $x$ = 0.03 showing the submicron grain size. b) TEM micrograph (unheated sample) showing a tetragonal domain structure in a proportion of the grains. Other non-domain structured grains may be pseudocubic, or tetragonal at differing orientations.**

### 3..2 Dielectric, Ferroelectric and Piezoelectric Properties

Unpoled KBT shows an inflection in the $\varepsilon_r$-T plots well below the peak temperature, $T_m$. There are reports in the research literature that this type of inflection in a relaxor represents its depolarisation temperature. Alternatively it has been suggested that a changeover from ferroelectric non-ergodic to ergodic state (non-ferroelectric) below the true depolarisation temperature is responsible. The results described below are consistent with the latter interpretation. Unpoled KBMT ceramics show no such inflection[31,32] but poling was found to induce a weak inflection, starting at ~150-170 °C (heating cycle), Figure 4. Thus an electric field stimulus is required to generate ferroelectric character in the non-ergodic regime for KBMT but unmodified KBT spontaneously transforms to ferroelectric. The weak nature of the

inflection in KBMT leads to uncertainty as to its true onset temperature. However the loss tangent plot for x = 0.03 shows a more noticeable discontinuity: values begin to rise on the heating cycle at temperatures above ~150°C reaching a broad maximum at ~220°C (1 kHz); this peak temperature in tanδ is similar to the depolarisation temperature $T_d$ obtained from charge decay measurements, confirming the tan δ data to be a reliable indicator of $T_d$.[31,32] The depolarisation of KBMT occurs at ~220°C, which is significantly higher than the $T_d$ of NBT-BT based piezoceramics.[5,19-21,36].

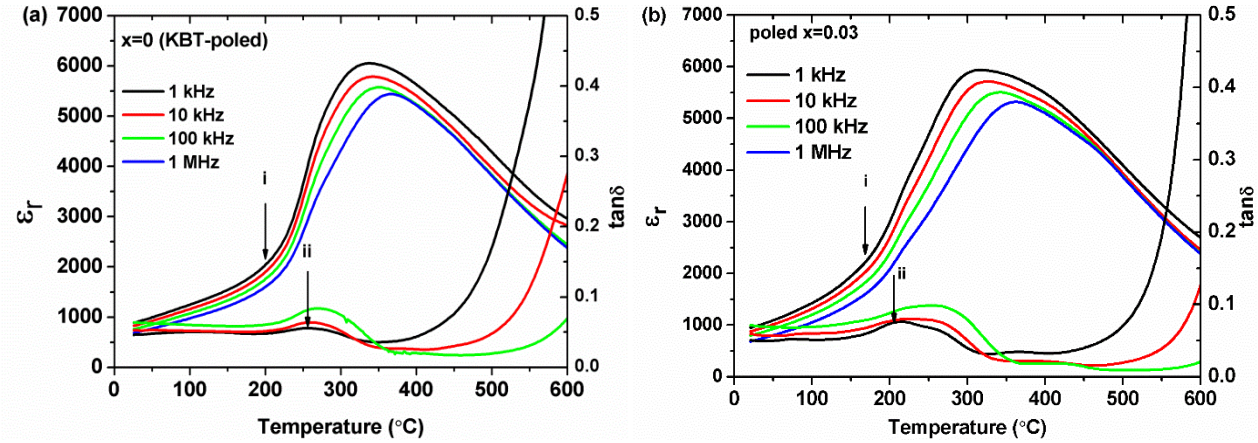


**Figure 4. Relative permittivity and loss tangent versus temperature for a) $x$ = 0 (KBT-poled), b) $x$ = 0.03-poled (arrow indicates the onset temperature of the inflection in (i) $\varepsilon_r$ and (ii) tanδ due to the changeover from ferroelectric to ergodic relaxor on heating. The peak in tanδ at ~ 220° C correlates with the depolarisation temperature.** [32]

Polarisation-electric field (P-E) measurements for mixed-phase $x$ = 0.03 KBMT show broad ferroelectric hysteresis loops at 25 °C, Figure 5. At higher temperatures the loops become narrower, which is consistent with the thermally-induced contraction in $c/a$ ratio of the tetragonal phase (Figure S3) and a resultant lowering of the coercive field, $E_c$. Remnant polarisation, $P_r$, values are ~ 20 μC/cm$^2$ at temperatures between 25 °C and 125 °C, reducing to ~15 μC/cm$^2$ at 150 °C. A change in the shape of the P-E loops occurs at 175 °C due to constriction and partial loss of polarisation at low fields, with $P_r$ reducing to ~10 μC/cm$^2$. For the single-phase tetragonal parent KBT material, no ferroelectric P-E response was observed at temperatures from 25 °C to 100 °C, indicating that a higher energy is required to initiate domain wall movement than is the case for KBMT, even though the $c/a$ ratios are only marginally different (Table 1).

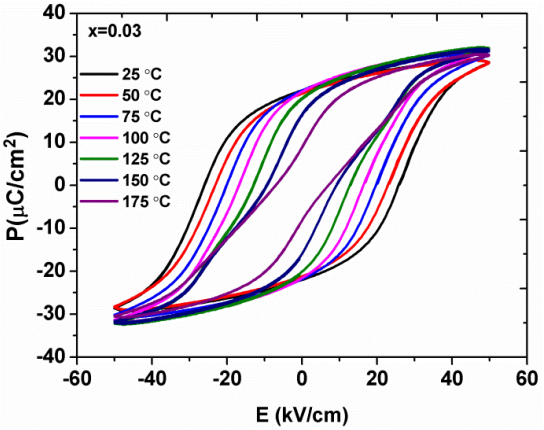


**Figure 5. Polarization-electric field loops as a function of temperature for $x$ = 0.03 (50 kV/cm) showing partial constriction at 175°C due to loss of low-field polarisation resulting from the onset of the change from ferroelectric to ergodic relaxor.**

The $x$ = 0.08 composition, which is single phase cubic according to the SXPD results, exhibits a ferroelectric P-E loop (Figure S4, Supporting Information). This indicates the occurrence of a field induced transition which is confirmed by *in situ* synchrotron XRD (as described below). Thus it is more accurate to refer to the 'cubic' phase as *pseudocubic* since its symmetry is field-dependent.

The temperature-dependence of the nonlinear dielectric properties was evaluated by analysis of P-E loops obtained from measurements in the sub-coercive field region, from 1 to 20 kV/cm, over a range of temperatures from 25 to 150°C. The results presented in Figure 6 for $x$ = 0.03 KBMT show that the dielectric permittivity values increase in a linear fashion with increasing field amplitude in accordance with the empirical Rayleigh law, which is typical for many ferroelectrics.[38] The Rayleigh coefficients, $\alpha'$, representing the gradient of the $\varepsilon_r$-T plots, increase with increasing temperature as a result of the increasing extrinsic (domain wall) contribution to permittivity. For example, for $x$ = 0.03 KBMT, the value of $\alpha'$ increases from 0.32 x $10^{-3}$ to 1.06 x $10^{-3}$ m/V as the temperature increases from 25°C to 150°C. At room-temperature, these Rayleigh coefficients are significantly lower than those of soft PZT (5.6 x $10^{-3}$ m/V) and are comparable to those of hard PZT (0.67 x $10^{-3}$ m/V).[39,40] This result is in accord with the relatively high coercive fields of KBMT ceramics at room-temperature.

The loss tangent values measured from the P-E loops in the sub-coercive field region also increase progressively as a function of increasing field amplitude and temperature, as illustrated in Figure 5. The trends in tanδ are similar to those obtained for $\varepsilon_r$. Although the loss tangent values reported here for the KBMT ceramics seem relatively high, it should be noted that these represent the 'high field' values and they are in fact comparable with those of soft PZT ceramics reported by Hall.[39,40] In general, the nonlinear dielectric properties of the KBMT ceramics in the temperature range from 25 to 150 °C conform to those

of a conventional ferroelectric ceramic. Further deviations from this behaviour are anticipated at higher temperatures due to the decay of the long range-ordered ferroelectric state.

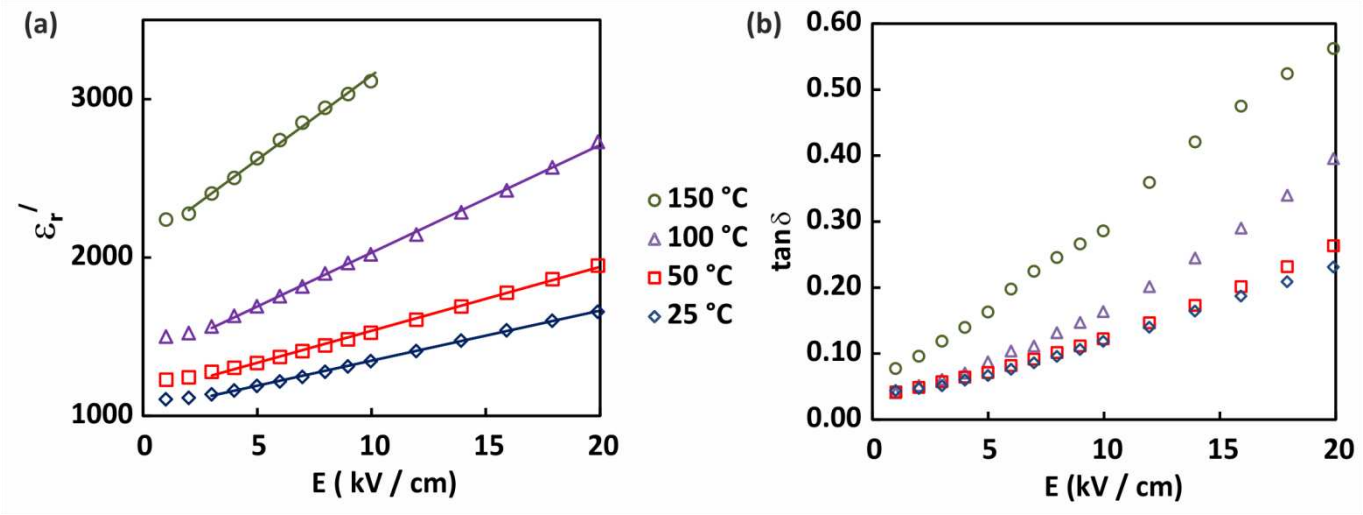


**Figure 6. a) Nonlinear dielectric permittivity, and b) loss tangent data for $x = 0.03$ ceramics measured over a range of electric field amplitudes and temperatures**.

The compositional dependence of the *direct* piezoelectric coefficient $d_{33}$ (measured by the Berlincourt method) is illustrated in Figure 7. A sharp increase in $d_{33}$ occurs between $x = 0.02$ and 0.03, giving a value of 150 pC/N for $x = 0.03$, then it reduces with further increases in BMT content. The maximum $d_{33}$ values lie within the upper range reported for NBT-BT and NBT-KBT ceramics,[5] No phase boundary was induced at x = 0.03 by the application of an electric field, confirming that $d_{33}$(max) is independent of a phase transition.

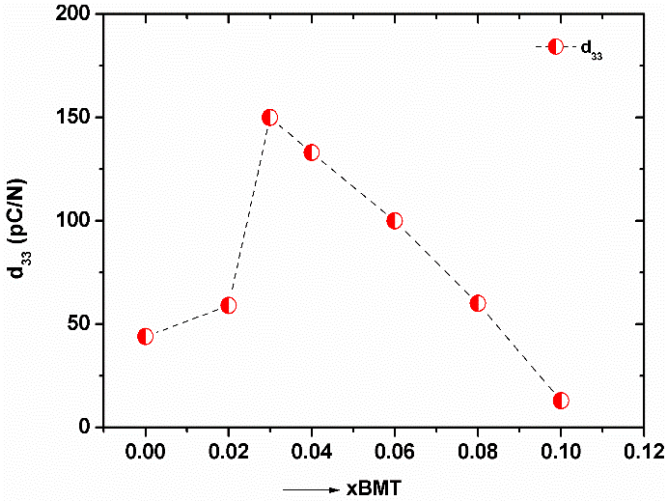


**Figure 7. Variation of piezoelectric charge coefficient, $d_{33}$, versus $x$ for the KBMT system.**

The $x = 0.03$ KBMT sample showed a two-fold increase in electric field-induced strain relative to $x = 0$ KBT, giving a value of 0.11 %, which is ~ 25% lower than that for a commercial hard PZT 806 (50 kV/cm, 1 Hz), as illustrated by the results presented in Figure 8. Increasing the field level to 80 kV/cm (at 1 Hz) results in a strain of 0.3% for KBMT; this compares to a 'giant' strain of 0.45% (at a much lower measurement frequency of 50 mHz) reported for NBT-BT-NKN ceramics under a comparable field.[26] For a field amplitude of 20 kV/cm, which is below $E_c$, a strain of 0.06% was recorded for $x = 0.03$ (Figure S6, Supporting Information).

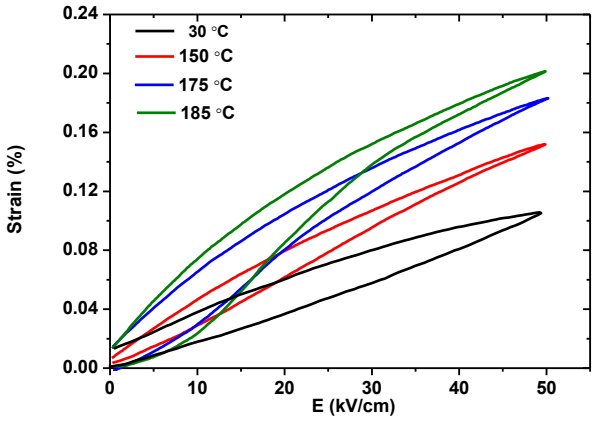


**Figure 8. Unipolar S-E loops for $x = 0.03$ showing elliptical loops with low hysteresis for temperatures up to 150 °C followed by a change in shape at 175 °C and 185 °C with increased hysteresis (span in S values).**

With increasing temperature the unipolar field-induced strains of x = 0.03 increase linearly from 0.11 - 0.14%, as temperature increases to 150 °C, with low hysteresis in strain values, Figures 8 and 9(a). The relatively low hysteresis (span in S values) and near-linearity in the S-E relationship with increasing temperature up to 150 °C (Figure S6), are distinctive in the field of Pb-free piezoelectrics. The temperature dependence of the unipolar S-E response equates to a consistent variation in strain of 3 x $10^{-4}$ % per °C. This linearity represents the behaviour of the ferroelectric non ergodic state; there is no evidence of temperature- or electric field-induced phase transitions between 20 and 150 °C.

At 175 °C and 185 °C there is a change in shape of the S-E loops, Figure 8, which translates to a steeper $S_{max}$-T plot, Figure 9a, with S reaching ~0.2% at 185 °C. The S-E loops were relatively narrow and elliptical at ≤ 150 °C but change at higher temperatures to broader loops (higher hysteresis) and with a discontinuity (bulge) on the up-field cycle, Figure 8. This change in the S-E relationship is attributed to the change to ergodic relaxor characteristics above 150 °C and a reversible field-induced transformation into the ordered ferroelectric state.

Trends in the effective high-field $d_{33}^*$ ($S_{max}/E_{max}$) values with temperature for x = 0.03 are presented in Figure 9b, and the strain-field maximum hysteresis values in Figure 9c. A slight decrease in hysteresis between 120 °C and 150 °C is consistent with a reduction in energy barrier of tetragonal domain wall movement due to a lower $E_c$ as the *c*/*a* tetragonal distortion decreases. Measured strain hysteresis values are 0.02-0.025% (absolute) for temperatures up to 150 °C, which compare favourably to other lead-free piezoelectrics.[5] The occurrence of the field-dependent transition causes $S_{max}$ and hysteresis in the S-E relationship to increase at temperatures above 150 °C, giving a hysteresis of 0.035% at 175°C and ~0.05% at 185 °C .

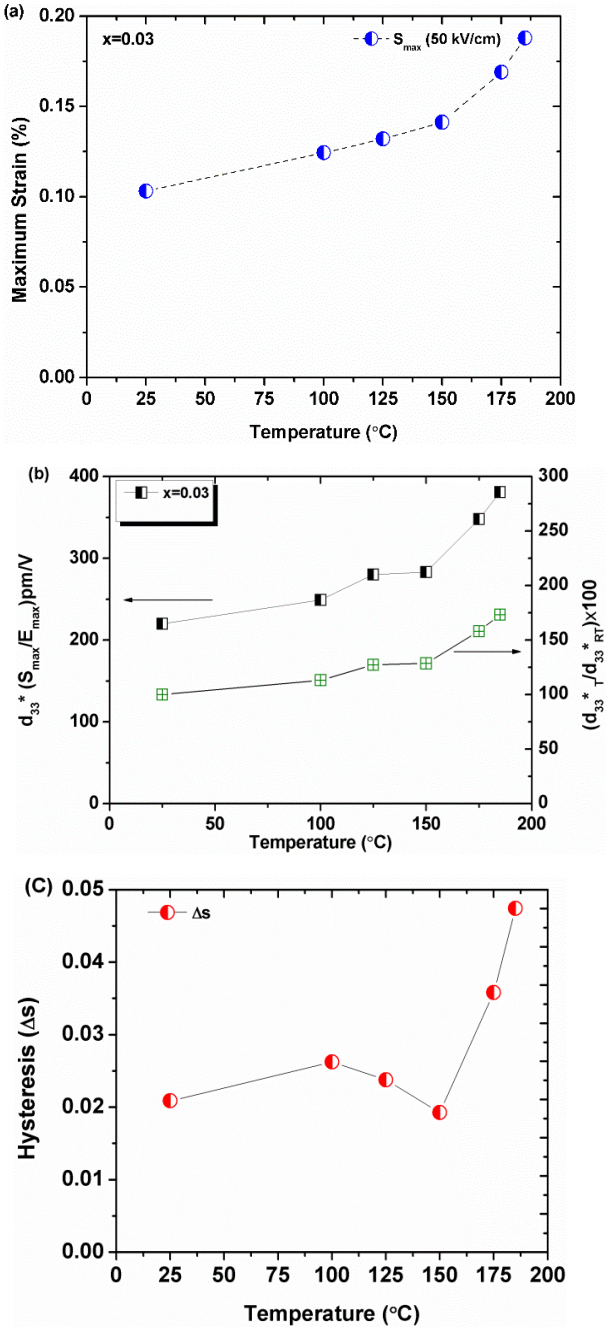


**Figure 9. a) Temperature-dependent unipolar strain, $S_{max}$, at 50 kV/cm (1 Hz), b) temperature variation of effective $d_{33}$* ($S_{max}/E_{max}$) and normalized values, $d_{33}$*T/$d_{33}$*$_{RT}$ c) strain maximum hysteresis (absolute) versus temperature, for the x = 0.03 composition.**

### 3.3 In-situ Synchrotron X-ray Diffraction

The potential contributions of electric field-induced phase transformations to the electro-mechanical behaviour of KBT-BMT ceramics were investigated further by conducting in-situ high-energy x-ray diffraction experiments. For x = 0.3, the diffraction patterns obtained at temperatures of 100 °C and below indicated the presence of coexisting tetragonal and pseudo-cubic phases, consistent with the results shown in Figures 1 and 2. In contrast, at a higher temperature of 150 °C the initial zero-field pattern corresponded to a single pseudo-cubic phase, as shown in Figure 10. This was found to transform into a mixture of pseudo-cubic and tetragonal phases, with phase fractions of approximately 63% and 37% respectively, at an electric field above 20 kV/cm. These results confirm the presence of a substantial volume fraction of non-ergodic PNRs for this composition at 150 °C, which transform irreversibly into the long-range ordered ferroelectric state upon poling. Similar observations of an irreversible electric field-induced transformation were also made for the x = 0.8 composition at room temperature, which explains the ferroelectric P-E loop of this pseudocubic composition (Figure S4). Laboratory XRD analysis of crushed sintered pellets of x = 0.03 indicated tetragonal phase persisted to ~260°C ( Figure 2) ; this disparity is associated with the effects of grinding and release of matrix constraint.

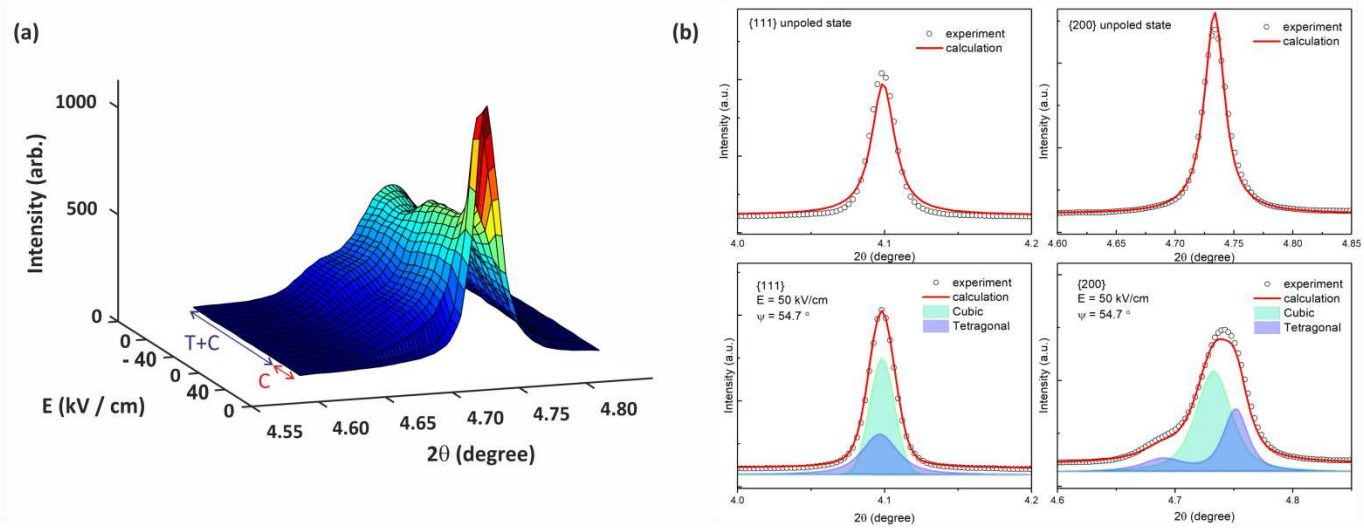


**Figure 10. (a) Changes in $\{200\}_p$ diffraction peak profiles and (b) full-pattern fitting obtained from in-situ high energy XRD measurements under a cyclic electric field up to 40 kV/cm at 150°C. Full-pattern fits were conducted at an azimuthal angle, ψ, of 54.7°, which is assumed to represent the strain- and texture-free state [41,42].**

## 4. Discussion

Within the compositional range $0 \leq x \leq 0.07$, the distinctive property trends in KBT-BMT arise for the following reasons: (a) co-existence of ferroelectric tetragonal and weakly polar pseudocubic phases which vary in relative proportion with changing overall composition, x; (b) a structural transformation from mixed to single phasepseudo cubic on heating which can be reversed by application of an electric field.

The highest $d_{33}$ value occurs in the two phase field at a phase ratio of approximately 50/50 tetragonal/pseudocubic, corresponding to solid solution composition $x = 0.03$. Powder X-ray diffraction of samples prepared from crushed sintered pellets shows the transition to single phase cubic at 260 °C (Figure 2) but corresponding synchrotron data on dense ceramic pellets indicates only pseudocubic phase can be detected at ~150°C (Figure 10). This points to phase stability and temperature range of stability of tetragonal KBMT being influenced bv microstructural matrix constraint effects.

Rietveld refinements point to a slightly higher Mg B-site occupancy in the pseudocubic phase (Table S1, Supplementary Information). Magnesium ions are known to be ferroelectrically inactive relative to titanium ions in a perovskite lattice. The higher Mg levels in pseudocubic KBMT would inhibit coherent long range polar order. However inferred compositional discrepancies between the two phases are below the detection limits of energy dispersive X-ray spectroscopy (EDX) using SEM or TEM analytical techniques.

The changes to polar length scales at ~ 150°C are responsible for a weak inflection in in $\varepsilon_r$-T plots of poled samples of KBMT and an increase in tan δ. However, full depolarisation ($T_d$) of $x = 0.03$ is not observed until ~ 220°C and is signified in Figure 4 by a peak in tan δ. [32] Further heating results in a characteristic frequency-dependent dielectric relaxation peak due to the changing dynamics of dipole coupling under an a.c. field.

The temperatures at which P-E loops of ceramic pellets begin to show constriction (Figure 5) due to the non-ergodic to ergodic changeover are consistent with the structural transition temperature identified by synchrotron X-ray diffraction. In P-E loop measurements at 175 °C and 185 °C, a reduction in polarisation at low fields is a consequence of the thermally induced change to weakly polar ergodic structure: at sufficient electric field the ferroelectric structure re-forms. The overall effect is P-E constriction.

The S-E loops show a change in shape above 150°C for a similar reason. The electric field-induced reverse transition of the ergodic to ferroelectric structure at 175°C or 185 °C creates an additional strain contribution. Thus the slope of the $S_{max}$ vs. T plots increases above 150 °C and a relatively high strain of ~

0.2% can be realized at 185 °C (the maximum temperature of the silicone oil bath). The time dependence of loss, or partial loss of field-induced long range order in KBMT after removal of the field is not known at this stage. Other Pb-free piezoceramics show evidence of field induced transitions in S-E response but for different reasons. For example, a field induced transition from mixed tetragonal and rhombohedral ferroelectric phases to a relaxor phase is reported at ambient temperatures for NKN-modified NBT-BT or NBT-KBT.[5,44]

The structure-property relationships in KBMT illustrate that in contrast to other piezoelectric perovskite solid solutions neither a MPB nor a PPT is involved in maximising piezoelectric performance. Thus traditional concepts of polarisation rotation between two ferroelectric phases of differing symmetry, e.g. tetragonal and rhombohedral, as being a pre-requisite to minimise the energy barrier for domain wall movement and achieve enhanced performance in a piezoelectric solid solution appear not to apply to KBMT. Instead, the key determinant is a varying proportion of transformable weakly polar pseudocubic phase, coexisting with a ferroelectric tetragonal phase.

We attribute the enhancement in piezoelectric performance of KBMT (x= 0.03) relative to unmodified KBT to a reduction in energy barrier for ferroelectric domain wall movement in the tetragonal crystallites due to the beneficial effect of the co-existing transformable pseudocubic crystallites. The proportion of pseudocubic phase increases with increasing x (Table 1), having a value of 52 % $x = 0.03$ (unpoled). The result is a ~ 3 fold increase in $d_{33}$ of poled samples relative to KBT at a ~ 50/50 ratio of each phase in KBMT. The explanation for this optimal ratio may relate to statistical probability of tetragonal and pseudocubic crystallites being intimately mixed. Local stress relief of dipole reorientation in tetragonal crystallites would be facilitated by adjacent pseudocubic crystallites. In KBT all crystallites are tetragonal with a moderately high *c/a* ratio, making reorientation of dipoles energetically unfavourable (at ambient temperatures) due to microstructural clamping, giving a linear P-E response. The pseudocubic phase reduces this constraint and makes it easier for domains to re-orientate thereby enhancing extrinsic piezoelectric contributions, most effectively at a 50/50 ratio. The dilution of the tetragonal component below a level of 50 % for x > 0.03 acts to lower $d_{33}$ values. A progressive reduction in c/a ratio as x increases would also be anticipated to lower the energy for domain realignment, at the expense of reduce intrinsic contributions. However the composition-property trends across the range of solid solutions studied point to phase-proportion as being the dominant factor.

In terms of property comparisons with other Pb-free piezoelectrics that retain performance to elevated temperatures, the best systems are the ferroelectric ceramics, (Na,K,Li)(Nb,Ta)$O_3$-$CaZrO_3$ [NKLNT-CZ], (Na,K,Li)$NbO_3$-$CaZrO_3$ [NKLN-CZ], and $Na_{0.5}K_{0.5}NbO_3$-$BaZrO_3$-(Bi,Li)$TiO_3$ [NKN-BZ-BLT].[9,10,45,46] Compositional modifications of the base NKN composition in these systems favourably modify the temperature of a PPT, and in some cases creates a more diffuse PPT. In the original example of

NKLNT-CZ, core-shell microstructures have an important bearing on properties, but no such segregation was evident from our TEM-EDX analysis of KBMT. Both NKLN-CZ and NKN-BZ-BLT have higher $d_{33}$ values than KBMT. However the maximum field-induced strains in KBMT are comparable to, or slightly higher than NKLN-5CZ, as is the depolarisation temperature ($T_d$ is just below 200 °C in NKLN-0.05CZ as opposed to 220 °C for KBMT), whilst the 'giant' strains of ~ 0.4% at 40 kV/cm reported for NKLNT-CZ are higher than for KBMT.[46] The highest measurement temperature in this work, ~ 185 °C, gives strains of ~0.2%. There is no PPT in the temperature range of strain measurements (20-185 °C) for KBMT. The damaging consequences of a PPT on piezoelectric response after repeated thermal cycling through the phase transition has been reported for NKN-LT[7]. The diffuse nature of the PPT in NKLN-0.05CZ at temperatures slightly above room-temperature is such that although strains initially increase then decrease on heating above 25 °C, they vary by only ± 10% of their room-temperature value (~ 0.13% at 40 kV/cm) up to a temperature of 175 °C[10] ($T_c$ is < 200°C) in single cycle measurements. This compares to a ~30% linear increase in $S_{max}$ for KBMT (to 150 °C); a number of commercial PZTs also exhibit a linear change in $S_{max}$ with temperature. In contrast to the linear increase in strain with temperature for KBMT, strains in NKN-BZ-BLT decrease in a non-linear manner on heating from 25 °C to 150 °C.[44]

## 5. Conclusions

Structure-property relationships have been investigated for the ceramic system $(1-x)K_{0.5}Bi_{0.5}TiO_3$-$xBi(Mg_{0.5}Ti_{0.5})O_3$. In contrast to traditional lead-containing or lead-free piezoceramics, optimum properties do not correspond to a morphotropic or polymorphic phase boundary. A maximum value of $d_{33}$ piezoelectric charge coefficient occurs at x = 0.03, which lies within a mixed phase tetragonal and pseudocubic region of the phase diagram at an approximately ~50:50 phase ratio. Anomalies in dielectric, ferroelectric and electromechanical properties at temperatures ≥150 °C in KBMT can be explained by a thermally induced transition from non-ergodic ferroelectric tetragonal to weakly polar ergodic relaxor state. Tetragonal KBMT can be regenerated by application of an electric field as confirmed by *in situ* synchrotron X-ray diffraction, a finding which explains the observed constriction in P-E loops and asymmetry in S-E loops at ≥ 150 °C.

## Conflict of interest

There are no conflicts of interest to declare.

**Acknowledgements**

Aurang Zeb thanks the Higher Education Commission of Pakistan and Islamia College Peshawar (Chartered University) for financial support. We wish to thank Research Councils UK for contributions to funding (EP/P015514/1) and thank the Diamond Light Source for access to beamline I11 (EE14322) that contributed to the results presented here. At Tsinghua University, this work was partially supported by the National Natural Science Foundation of China (Grant No. 51332002). Thanks are also expressed to Andrew Bell, Tim Comyn, James Bennett and other colleagues at Leeds for valuable advice.

**References**

(1) B. Jaffe, W. R. Cook, H. Jaffe, Piezoelectric ceramics; Academic Press: London, 1971.

(2) B. Noheda, D. E. Cox, G. Shirane, G. A. Gonzalo, L. E. Cross, S. E. Park, Appl. Phys. Lett., 74, (1999) 2059-2061.

(3) R. C. Turner, F. A. Fuierer, R. E. Newnham, T. R. Shrout, Appl. Acoust, 41 (1994) 299-324.

(4) T. Y. Ansell, D. P. Cann, E. Sapper, J. Rödel, J. Am. Ceram. Soc., 98 (2015) 455-463.

(5) J. Rödel, W. Jo, K. T. P. Seifert, E. M. Anton, T. Granzow, D. Damjanovic, J. Am. Ceram. Soc., 92 (2009) 1153-1177.

(6) Y. Guo, K. I. Kakimoto, H. Ohsato, Appl. Phys. Lett., 85 (2004) 4121.

(7) T. A. Skidmore, T. P. Comyn, S. J. Milne, Appl. Phys. Lett., 94 (2009) 222902.

(8) J.-F Li, K. Wang, F.-Y. Zhu, L. Q. Cheng, F.-Z. Yao, J. Am. Ceram. Soc., 96 (2013) 3677-3696.

(9) R. Wang, H. Bando, M. Itoh, IMF-ISAF Conf. Xi'an, China, 2009, DO-033.

(10) K. Wang, F.-Z. Yao, W. Jo, D. Gobeljic, V. V. Shvartsman, D. C. Lupascu, J.F. Li, J. Rödel, J. Adv. Funct. Mater., 23 (2013) 4079-4086.

(11) T. A. Skidmore, T. P. Comyn, A. J. Bell, F. Y. Zhu, S. J. Milne, IEEE Trans. Ultrason. Ferroelectr. Freq. Control, 58 (2011) 1819.

(12) K. Wang, J.-F. Li, J. J. Zhou, Appl. Phys. Express, 4 (2011) 061501.

(13) T. Takenaka, K.-I. Maruyama, K. Sakata, Jpn. J. Appl. Phys., , 30 (1991) 2236-2239.

(14) Y. Guo, Y. Liu, R. L. Withers, F. Brink, H. Chen, Chem. Mater., 23 (2011) 219-228.

(15) W. Jo, J. E. Daniels, J. L. Jones, X. Tan, P. A. Thomas, D. Damjanovic, J. Rödel, J. Appl. Phys., 109 (2011) 014110.

(16) C. Ma, X. Tan, E. Dul'kin, M.J. Roth, J. Appl. Phys., , 108 (2010) 104105.

(17) I. Levin, I. M. Reaney, E. M. Anton, W. Jo, J. Rödel, J. Pokorny, L. A. Schmitt, H.-J. Kleebe, M. Hinterstein, J. L. Jones, Phys. Rev. B 87 (2013) 024113.

(18) Y.-R. Zhang, J.-F. Li, B.-P. Zhang, C.-E. Peng, J. Appl. Phys., , 103 ( 2008) 074109.

(19) K. Yoshii, Y. Hiruma, H. Nagata, T. Takenaka, Jpn. J. Appl. Phys., 45(5B) (2006) 4493-4496.

(20) Y. Hiruma, H. Nagata, T. Takenaka, J. Appl. Phys., 104 (2008) 124106.

(21) A. J. Royles, A. J. Bell, A. P. Jephcoat, A. K. Kleppe, S. J. Milne, T. P. Comyn, Appl. Phys. Lett., 97 (2010) 132909.

(22) H. Simons, J. E. Daniels, J. A. Glaum, A. J. Studer, J. L. Jones, M. Hoffman, Appl. Phys. Lett., 102 (2013) 062902.

(23) E.-M. Anton, W. Jo, D. Damjanovic, J. Rödel, J. Appl. Phys., 110 (2011) 094108.

[24] Y. Hiruma, Y. Makiuchi, R. Aoyagi, H. Nagata, T. Takenaka, Ceram. Trans., 174 (2005) 139.

(25) H. Nagata, M. Yoshida, Y. Makiuchi, T. Takenaka, Jpn. J. Appl. Phys., 42 (2003) 7401-7403.

(26) S.-T. Zhang, A. B. Kounga, E. Aulbach, T. Granzow, W. Jo, H.-J. Kleebe, J. Rödel, J. Appl. Phys., 103 (2008) 034107.

(27) J. E. Daniels, W. Jo, J. Rödel, V. Honkimäki, J. L. Jones, Acta Mater., 58 ( 2010) 2103-2111.

(28) J. Hao, B. Shen, J. Zhai, H. Chen, J. Appl. Phys., 115 (2014) 034101.

(29) H. Nagata, K. Tabuchi, T. Takenaka, Jpn. J. Appl. Phys., 52 (2013) 09KD05.

(30) Y. Hiruma, R. Aoyagi, H. Nagata, T. Takenaka, Jpn. J. Appl. Phys., 44 (2005) 5040-5044.

(31) A. Zeb, S. J. Milne, J. Am. Ceram. Soc., 97 (2014) 2413-2415.

(32) A. Zeb, D. A. Hall, S. J. Milne, J. Mater. Sci.: Mater. Electron., 26 (2015) 9516-9521.

(33) P. Jaita, P. Jarupoom, R. Yimnirun, G. Rujijanagul, D. P. Cann, Ceram. Int., 42 (2016) 15940-15949.

(34) S. P. Thompson, J. E. Parker, J. Potter, T. P. Hill, A. Birt, T. M. Cobb, F. Yuan, C. C. Tang, Review Sci. Inst., 80 (2009) 075107-1.

(35) A. C. Larson and R. B. Von Dreele, Los Alamos National Laboratory Report No. LAUR 86-748, 2004 (unpublished).

(36) M. Chen, Q. Xu, B. H. Kima, B. K. Ahn, J. H. Ko, W. J. Kang, O. J. Nam, J. Eur. Ceram. Soc., 28 (2008) 843-849.

(37) B. Wylie-van Eerd, D. Damjanovic, N. Klein, N. Setter, J. Trodahl, J. Phys. Rev. B, 82 ( 2010) 104112.

(38) D. A. Hall, M. M. Ben-Omran, P. J. Stevenson, J. Phys: Condens. Matt., 10 (1998), 461-476.

(39) D. A. Hall, J. Mater. Sci., 36 (2001) 4575-4601.

(40) D. A. Hall, Ferroelectrics, , 223 (1999) 319-328.

(41) D.A. Hall, A. Steuwer, B. Cherdhirunkorn, P.J. Withers, T. Mori, J. Mech. Phys. Solids 53 (2005) 249-260

(42) J. Filik et al., J. Appl. Cryst. 50 (2017) 959-966

(43) T. Roncal Herrero, J. Harrington, A. Zeb S. J. Milne, A. P. Brown, Acta Materialia 158 (2018) 422-429

(44) W. Jo, T. Granzow, E. Aulbach, J. Rödel, D. Damjanovic, J. Appl. Phys., 105 ( 2009) 094102.

(45) S.-Y. Choi, S. J. Jeong, D.-S. Lee, M.-S. Kim, J.-S. Lee, J. H. Cho, B. I. Kim, Y. Ikuhara, Chem. Mater., 24 (2012) 3363.

(46) R. Wang, K. Wang, F. Yao, J. F. Li, F. H. Schader, K. G. Webber, W. Jo, J. Rödel, J. Am. Ceram. Soc.,, 98, (2015) 2177-2182.

*SUPPLEMENTARY INFORMATION*

**Table S1. Refined crystal structure for each composition**

x=0 Tetragonal

| Site | x | y | z | $U_{iso}$ (100 x Å$^2$) | Nominal occupancy | Refined occupancy |
|---|---|---|---|---|---|---|
| K (+1) | 0 | 0 | 0 | 3.02(2) | 0.5 | 0.507(3) |
| Bi (+3) | 0 | 0 | 0 | 3.02(2) | 0.5 | 0.493(3) |
| Ti (+4) | 0.5 | 0.5 | 0.4401(5) | 0.90(5) | 1 | 1.019(5) |
| O1 (-2) | 0.5 | 0.5 | -0.079(2) | 0.23(5) | 1 | 1.08(1) |
| O2 (-2) | 0.5 | 0 | 0.395(1) | 2.34(7) | 1 | 1.03(2) |

x=0.02 Tetragonal

| Site | x | y | z | $U_{iso}$ (100 x Å$^2$) | Nominal occupancy | Refined occupancy |
|---|---|---|---|---|---|---|
| K (+1) | 0 | 0 | 0 | 2.60(5) | 0.49 | 0.496(3) |
| Bi (+3) | 0 | 0 | 0 | 2.60(5) | 0.51 | 0.504(3) |
| Ti (+4) | 0.5 | 0.5 | 0.4385(4) | 2.12(6) | 0.99 | 0.992(3) |
| Mg (+2) | 0.5 | 0.5 | 0.4385(4) | 2.12(6) | 0.01 | 0.008(3) |
| O1 (-2) | 0.5 | 0.5 | -0.0805(6) | 0.14(8) | 1 | 1.03(7) |
| O2 (-2) | 0.5 | 0 | 0.4012(7) | 0.66(8) | 1 | 1.00(9) |

Cubic

| Site | x | y | z | $U_{iso}$ (100 x Å$^2$) | Nominal occupancy | Refined occupancy |
|---|---|---|---|---|---|---|
| K (+1) | 0 | 0 | 0 | 3.14(3) | 0.49 | 0.498(4) |
| Bi (+3) | 0 | 0 | 0 | 3.14(3) | 0.51 | 0.502(4) |
| Ti (+4) | 0.5 | 0.5 | 0.5 | 1.97(2) | 0.99 | 0.989(3) |

| | | | | | | |
|---|---|---|---|---|---|---|
| Mg (+2) | 0.5 | 0.5 | 0.5 | 1.97(2) | 0.01 | 0.011(3) |
| O1 (-2) | 0.5 | 0.5 | 0 | 3.3(6) | 1 | 0.98(8) |

ctd

Table S1

x=0.03 Tetragonal

| Site | x | y | z | $U_{iso}$ (100 x Å$^2$) | Nominal occupancy | Refined occupancy |
|---|---|---|---|---|---|---|
| K (+1) | 0 | 0 | 0 | 3.26(4) | 0.485 | 0.488(2) |
| Bi (+3) | 0 | 0 | 0 | 3.26(4) | 0.515 | 0.512(2) |
| Ti (+4) | 0.5 | 0.5 | 0.4561(8) | 1.35(3) | 0.985 | 0.991(3) |
| Mg (+2) | 0.5 | 0.5 | 0.4561(8) | 1.35(3) | 0.015 | 0.009(3) |
| O1 (-2) | 0.5 | 0.5 | -0.0639(3) | 5.78(6) | 1 | 1.000(3) |
| O2 (-2) | 0.5 | 0 | 0.4496(2) | 1.75(5) | 1 | 1.001(4) |

Cubic

| Site | x | y | z | $U_{iso}$ (100 x Å$^2$) | Nominal occupancy | Refined occupancy |
|---|---|---|---|---|---|---|
| K (+1) | 0 | 0 | 0 | 4.70(3) | 0.485 | 0.487(4) |
| Bi (+3) | 0 | 0 | 0 | 4.70(3) | 0.515 | 0.513(4) |
| Ti (+4) | 0.5 | 0.5 | 0.5 | 1.45(4) | 0.985 | 0.982(4) |
| Mg (+2) | 0.5 | 0.5 | 0.5 | 1.45(4) | 0.015 | 0.018(4) |
| O1 (-2) | 0.5 | 0.5 | 0 | 3.85(6) | 1 | 1.009(4) |

x=0.04 Tetragonal

| Site | x | y | z | $U_{iso}$ (100 x Å$^2$) | Nominal occupancy | Refined occupancy |
|---|---|---|---|---|---|---|
| K (+1) | 0 | 0 | 0 | 2.48(9) | 0.48 | 0.483(3) |

| | | | | | | |
|---|---|---|---|---|---|---|
| Bi (+3) | 0 | 0 | 0 | 2.48(9) | 0.52 | 0.517(3) |
| Ti (+4) | 0.5 | 0.5 | 0.566(1) | 1.56(5) | 0.98 | 0.991(3) |
| Mg (+2) | 0.5 | 0.5 | 0.566(1) | 1.56(5) | 0.02 | 0.009(3) |
| O1 (-2) | 0.5 | 0.5 | 0.060(8) | 4.99(8) | 1 | 1.01(1) |
| O2 (-2) | 0.5 | 0 | 0.618(2) | 1.84(4) | 1 | 1.03(2) |

Cubic

| Site | x | y | z | $U_{iso}$ (100 x Å$^2$) | Nominal occupancy | Refined occupancy |
|---|---|---|---|---|---|---|
| K (+1) | 0 | 0 | 0 | 3.64(9) | 0.48 | 0.483(3) |
| Bi (+3) | 0 | 0 | 0 | 3.64(9) | 0.52 | 0.517(3) |
| Ti (+4) | 0.5 | 0.5 | 0.5 | 1.39(7) | 0.98 | 0.972(2) |
| Mg (+2) | 0.5 | 0.5 | 0.5 | 1.39(7) | 0.02 | 0.028(2) |
| O1 (-2) | 0.5 | 0.5 | 0 | 3.40(2) | 1 | 0.992(4) |

ctd

Table S1

Tetragonal

x=0.07

| Site | x | y | z | $U_{iso}$ (100 x Å$^2$) | Nominal occupancy | Refined occupancy |
|---|---|---|---|---|---|---|
| K (+1) | 0 | 0 | 0 | 2.22(12) | 0.465 | 0.471(5) |
| Bi (+3) | 0 | 0 | 0 | 2.22(12) | 0.535 | 0.529(5) |
| Ti (+4) | 0.5 | 0.5 | 0.560(1) | 1.81(17) | 0.965 | 0.989(4) |
| Mg (+2) | 0.5 | 0.5 | 0.560(1) | 1.81(17) | 0.035 | 0.011(4) |
| O1 (-2) | 0.5 | 0.5 | 0.026(2) | 4.42(11) | 1 | 0.98(2) |
| O2 (-2) | 0.5 | 0 | 0.639(3) | 4.75(31) | 1 | 0.99(3) |

Cubic

| Site | x | y | z | $U_{iso}$ (100 x Å$^2$) | Nominal occupancy | Refined occupancy |
|---|---|---|---|---|---|---|
| K (+1) | 0 | 0 | 0 | 3.32(5) | 0.465 | 0.467(2) |
| Bi (+3) | 0 | 0 | 0 | 3.32(5) | 0.535 | 0.533(2) |
| Ti (+4) | 0.5 | 0.5 | 0.5 | 1.07(4) | 0.965 | 0.949(1) |
| Mg (+2) | 0.5 | 0.5 | 0.5 | 1.07(4) | 0.035 | 0.051(1) |
| O1 (-2) | 0.5 | 0.5 | 0 | 1.44(6) | 1 | 1.006(3) |

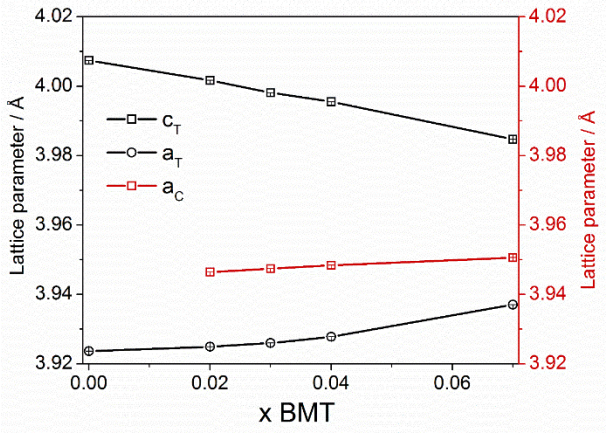


**Figure S1. Lattice parameters obtained from the Rietveld refinements of the high resolution synchrotron diffraction data.**

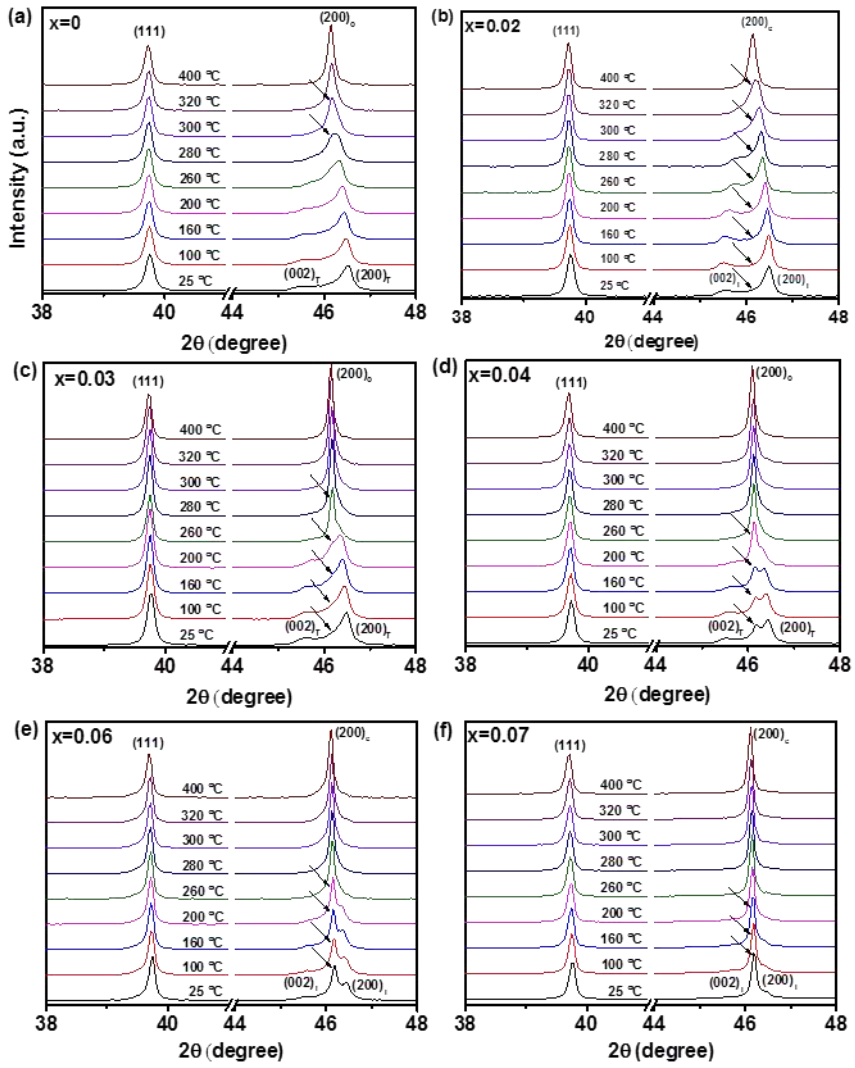


**Figure S2. High temperature X-ray diffraction patterns used to construct the phase diagram ( arrow indicates cubic 200 peak).**

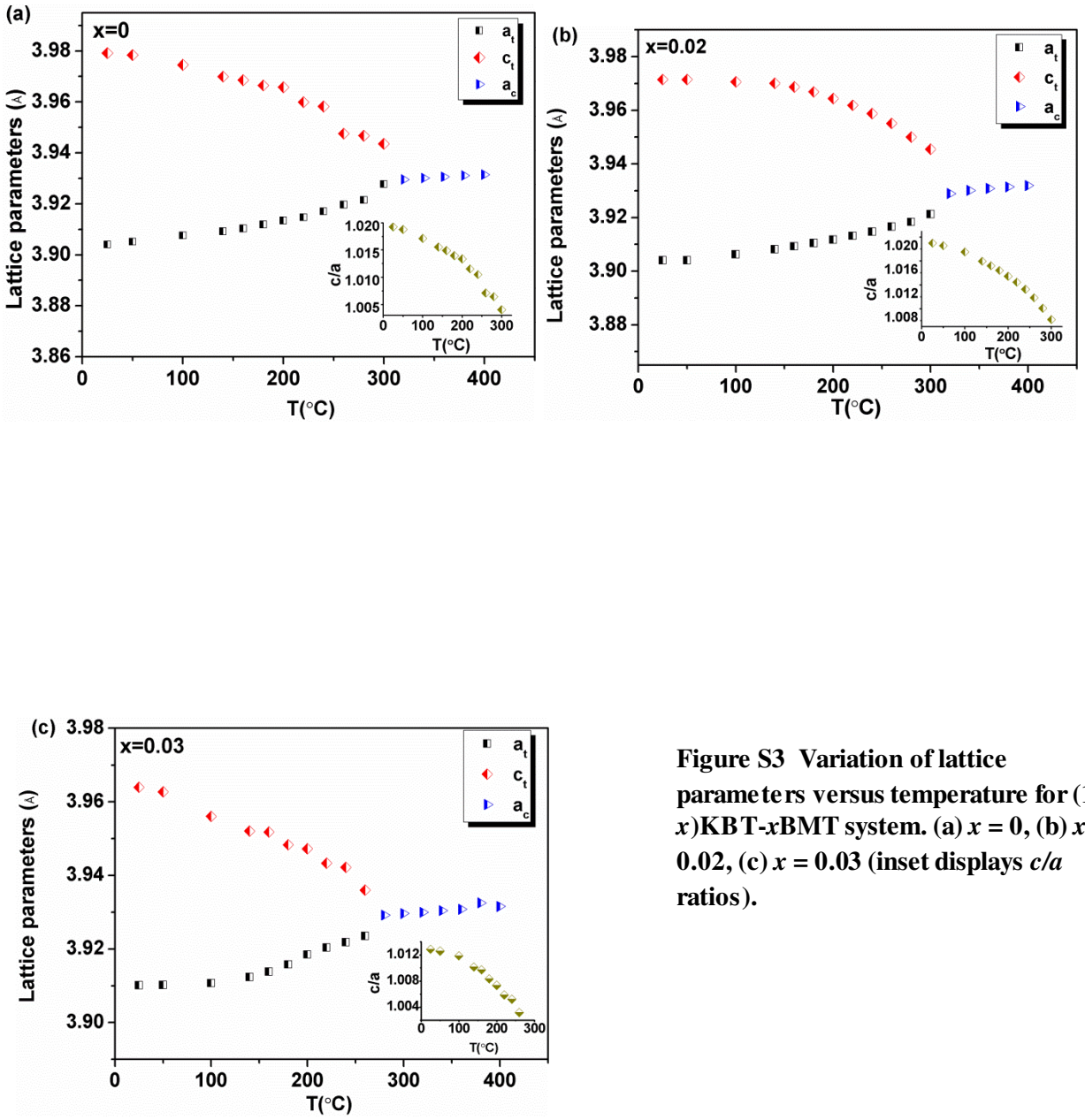


**Figure S3 Variation of lattice parameters versus temperature for (1-*x*)KBT-*x*BMT system. (a) *x* = 0, (b) *x* = 0.02, (c) *x* = 0.03 (inset displays *c/a* ratios).**

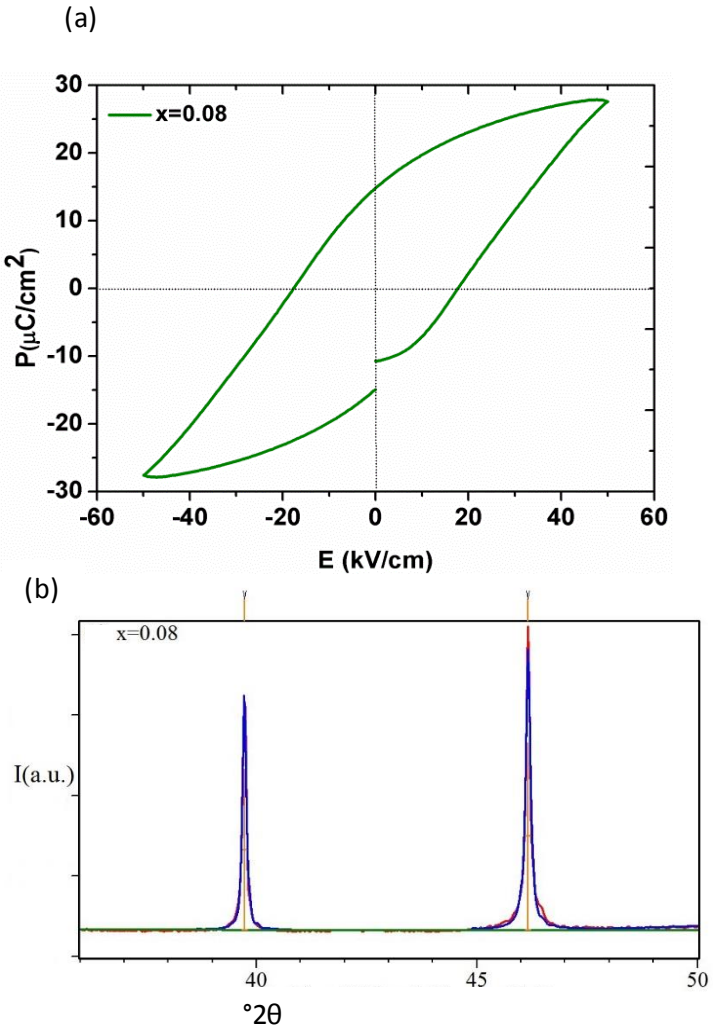


**Figure S4. (a) Polarisation-electric field loop (room-temperature) for x = 0.08 ; (b) XRD pattern highlighting the 111 and 200 reflections.**

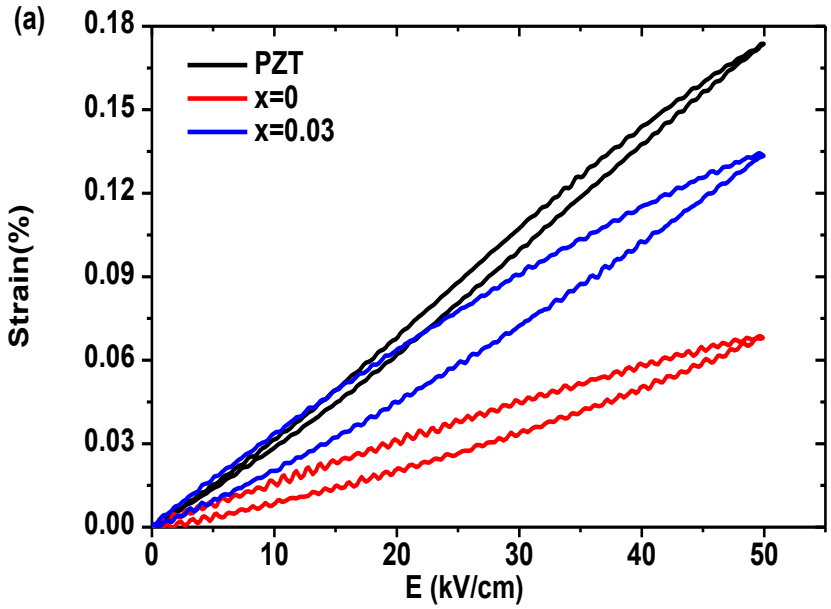


**Figure S5 Electric field induced strain (room-temperature) for x = 0, 0.03 and a *low-hysteresis* hard commercial PZT (PZT 806 Morgan Advanced Materials)**

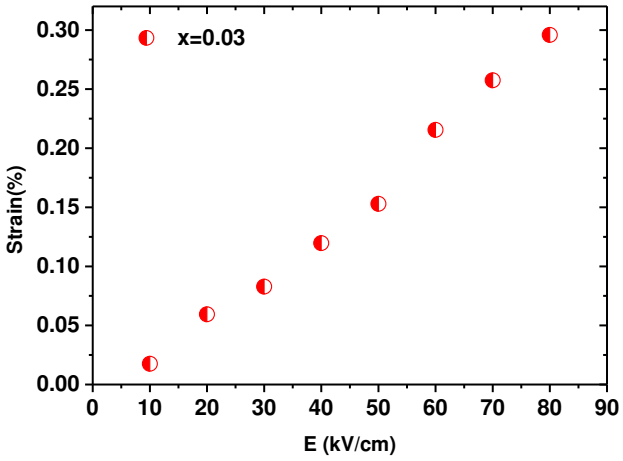


**Figure S6 Strain versus incremental electric field strength for x = 0.03**